Engineering Structures 268 (2022) 114724

Contents lists available at ScienceDirect

Engineering Structures

journal homepage: www.elsevier.com/locate/engstruct

Shear behaviour of beams strengthened using different Ni-Ti-Nb shape memory alloy wire configurations and design proposal based on the compression chord Capacity model (CCCM)

Joan M. Rius, Antoni Cladera, Benito Mas, Carlos Ribas *

Department of Industrial Engineering and Construction. University of Balearic Islands, Palma de Mallorca, Spain

ARTICLE INFO

Keywords:
Ni-Ti-Nb
Shape memory effect
Shear strength
Reinforced concrete
Strengthening

ABSTRACT

Shear strengthening of existing structures is often required in cases where shear strength is deficient because shear failures in RC members are associated with brittle collapse. In previous papers, the authors presented an innovative system for active strengthening shear critical-reinforced concrete (RC) beams using shape memory alloys (SMA) to take advantage of the shape memory effect. The authors also presented an approach to design this type of reinforcement based on the Compression Chord Capacity Model (CCCM). This model considers several shear transfer actions, including increased shear strength of the concrete compressed chord due to its confinement.

This article presents an experimental study of RC beams with new types of SMA strengthening systems that also improve the shear behaviour of beams.

The new types of tested shear strengthening systems are U-shaped external wires to facilitate the construction process by reducing initial imperfections; spiral active SMA wire implanted into a groove in the lower RC specimen part to see if it improves the dowel action effect; spiral active SMA wire only confining the compressed chord to check whether the CCCM predictions in this regard are adequate.

1. Introduction

Building structures and civil infrastructures undergo changes in use throughout their lifetime and extensions and/or modifications. The loads requested to structural elements are increased during many of these interventions. In addition, the stock of both reinforced concrete (RC) structures in buildings and civil infrastructures are ageing, which requires a maintenance programme that often crystallises in a specific or generalised structure retrofit. So it is becoming increasingly important to perform strengthenings to extend the lifetime of RC structures. This lifetime extension has become a primary environmental goal.

Shear failures of RC elements can also be fragile in some cases, which is the reason for the shear strengthening of RC structures to provide increased shear strength and improve ductility.

In recent years, different shear strengthening techniques have been studied using several materials and anchoring systems. Adhikary and Mutsuyoshi studied steel brackets, steel plates, vertical strips and externally anchored stirrups as effective retrofits for enhancing the shear strength of RC beams [1]. Due to their high strength-to-weight ratios and excellent durability, FRP composites have become widely used for retrofitting RC structures, including shear strengthening [2].

Active shear strengthening has also been studied using different materials: prestressed stainless-steel ribbons by Colajanni et al. [3], who confined in some tests only the partial depth of the cross-section of RC beams to simulate the usual RC beam condition below the floor slab; prestressed carbon fibre-reinforced polymer (CFRP) tested by Motavalli et al. [4] in EMPA laboratories for flexural and shear strengthening, and also for column confinement; and different SMAs in various forms.

The SMAs used for the shear strengthening of RC beams can be classified into two groups: iron-based SMA (Fe-SMA) [5–8] and Nickel-Titanium-Niobium SMA (Ni-Ti-Nb wires) [9]. The latter is related to this paper. Regarding iron-based alloys, the first active shear strengthening was studied for an actual application: in 2001, Soroushian et al. [5] tested a reinforced concrete beam strengthened with Fe-Mn-Si-Cr rods and then applied this technology to repair a bridge with shear cracks in Michigan, where the alloy developed recovery stresses of 255 MPa after heating it to 300 °C to, thus, mainly close a shear crack.

* Corresponding author at: Department of Industrial Engineering and Construction, University of the Balearic Islands. Ctra. Valldemossa, km 7.5, Palma (Balearic Islands), Spain.

E-mail address: carlos.ribas@uib.es (C. Ribas).

https://doi.org/10.1016/j.engstruct.2022.114724
Received 7 February 2022; Received in revised form 26 May 2022; Accepted 22 July 2022
Available online 30 July 2022

Nomenclature

a	shear span, the distance from the support to the resultant of the loads producing shear at that support.
b	width of the cross-section.
d	effective depth of the cross-section.
l	beam length
f_{cd}	is the design value of concrete compressive strength.
f_{ck}	characteristic compressive strength of concrete.
f_{cm}	mean compressive strength of concrete using 150-mm cubes.
$f_{cm,cyl}$	mean compressive strength of concrete using 150 × 300 mm cylinders, considered equal to $0.9f_{cm}$.
f_s	stress in the spiral or U-stirrup at failure, equal to $\sigma_R + \Delta\sigma_\varepsilon$, in previous works the steal yield stress.
f_{sp}	mean splitting strength of concrete using 150 mm × 300 mm cylinders.
f_y	mean yield strength of the reinforcement.
f_{ywd}	design yield strength of the shear reinforcement.
f_u	failure strength of the reinforcement.
h	overall depth of a cross-section.
i_0	percentage of initial imperfection of the wires.
s	spacing of the stirrups.
x	neutral axis depth of the cracked section, obtained assuming zero concrete tensile strength.
z	inner lever arm. In the shear analysis of reinforced concrete members without axial force, the approximate value $z \approx 0.9d$ may normally be used.
A_f	austenite finish temperature.
A_s	austenite start temperature.
A_{sw}	cross-sectional area of the shear reinforcement.
E_{cm}	secant modulus of elasticity of concrete, $E_{cm} = 22000(f_{cm}/10)^{0.3} \not> 39GPa$.
E_s	modulus of elasticity of reinforcing steel.
M_f	martensite finish temperature.
M_s	martensite start temperature.
V_{cu}	concrete contribution to the shear resistance of the member.
$V_{cu}^{confinement}$	increase of the concrete contribution to the shear resistance of the member due to confinement.
$V_{no\ strength.}$	average shear strength of not strengthened beams.
V_R	design shear resistance of the member.
$V_{R,\max}$	design value of the maximum shear force which can be sustained by the member, limited by crushing of the struts.
V_{su}	contribution of internal or external shear reinforcement to the shear resistance of the member.
V_{test}	experimental shear strength of a tested beam.
α	angle between shear reinforcement and the beam axis perpendicular to the shear force in Eq. (4) and Eq. (5).
α_{cw}	coefficient taking account the state of the stress in the struts: $\alpha_{cw} = 1$ for non prestressed structures; $\alpha_{cw} = 1 + \sigma_{cp}/f_{cd}$ for $0 \le \sigma_{cp} \le 0.25f_{cd}$; $\alpha_{cw} = 1.25$ for $0.25f_{cd} < \sigma_{cp} \le 0.50f_{cd}$; and $\alpha_{cw} = 2.5(1 - \sigma_{cp}/f_{cd})$ for $0.50f_{cd} < \sigma_{cp} \le f_{cd}$.
α_e	modular ratio, $\alpha_e = E_s/E_{cm}$.
δ	mid-span deflection
ν_1	strength reduction factor for concrete cracked in shear, $\nu_1 = 0.6$ for $f_{ck} \le 60$ MPa and $\nu_1 = 0.9\text{-}f_{ck}/200$ for $f_{ck} > 60$ MPa.
θ	angle between the concrete compression strut and the beam axis perpendicular to the shear force, given by Eq. (9).
ρ_l	longitudinal tensile reinforcement ratio referred to the effective depth d and the width b.
σ_R	recovery stress taking into account the initial imperfection i_0.
ζ	combined size and slenderness effect factor, given by Eq. (6).
Δ_{Vcu}	non-dimensional confinement factor which considers the increment of the shear resisted by the concrete caused by the stirrup confinement in the compression chord, see Eq. (4) and (8).
$\Delta\sigma_\varepsilon$	stress increase from the recovery stress in the Ni-Ti-Nb wires at shear failure of the strengthened beams.

More than one decade later, several researchers used another iron-based alloy (Fe-Mn-Cr-Ni) provided in strips for external active shear strengthening purposes. Zerbe et al. [6] applied it to RC T-beams and observed an increment in shear strength of around 20–25% on retrofitted beams. However, the anchorage system influenced the critical shear crack pattern, and the results were inconclusive. Montoya et al. [7] employed these strips to transversally prestress or confine the whole cross-section of 10 rectangular small-scale RC beams. They observed that the appearance of shear cracks was delayed for the retrofitted RC beams with activated strips. Cladera et al. [8] tested RC T-beams strengthened with different quantities of U-shaped strips and distinct anchoring configurations to observe an approximate 30% increase in the shear strength of retrofitted beams. However, these authors concluded that the need to anchor strips and the subsequent activation probably weakened the flange-web connection and hindered closing the shear truss, which would provide less ductile behaviour than expected. The same iron-based alloy used in the last cited works has also been employed for flexural strengthening in different circumstances [10–13].

Karayannis and Chalioris [14] in 2013 and Mas et a. in 2016 [15] studied the shear behaviour of rectangular spiral reinforcement, the former in steel and the latter in pseudoelastic Ni-Ti, as internal shear reinforcement of RC linear elements. They observed that this continuous stirrup type improved post-peak deformation ductility compared to the beams with an equal quantity of commonly used stirrups. The spiral configuration was also applied in [9], using SMA (Ni-Ti-Nb) wires capable of generating recovery stresses of up to 436 MPa as external active shear strengthening. It was concluded that by placing the SMA retrofit, the initial imperfections caused initial prestressing losses of the recovery stresses generated due to the shape memory effect (SME). Moreover, it was observed in [9] that the Compression Chord Capacity Model (CCCM) very suitably predicted both the beneficial effect of active shear strengthening and the favourable effect of confining the RC element core with no modification made to its original formulation. Besides all this, it was also found [9] that active strengthening could partially close cracks and increase both shear strength and ductility in shear failures.

The fact that the initial imperfections diminished the effectiveness of the initial prestressing, mainly due to the spiral strengthening geometry generating curvature of the wires (imperfections) at the upper and lower edges, is one reason why that research is herein continued, where new constructive solutions are proposed in this paper to reduce that degree of imperfection. The proposal is made to compare the behaviour of reinforcements with U-shaped stirrups anchored by steel plates to that of the continuous rectangular spiral used in [9]. Moreover, efforts were also made to improve the easiness of employing this strengthening system.

Furthermore, the good predictions achieved by the CCCM for SMA shear strengthened reinforced concrete beams presented in [9], and the

model's ability to predict the beneficial effect of compressed chord confinement [16] allowed the proposal of using an SMA spiral shear retrofit that wraps only the compressed chord. The study of such strengthening is twofold: on the one hand, it intends to verify the previously observed goodness of the CCCM model [9] in this sense because the initial model's hypothesis takes into account vertical stresses at the compression chord; on the other hand, it aims to evaluate whether a reinforcement of this style, such as that already proposed in [17] with very good results (albeit reinforcement was internal and passive in that case), is of economic interest.

2. Shear strength of RC structures

The shear strength of reinforced concrete (RC) beams is still a hot topic for the scientific community, and no general agreement on shear models has been reached. By way of example, the American Concrete Institute (ACI) did not change its 318 Building Code Guidelines for shear strength in reinforced concrete beams in about 50 years, and when it did, it based the code shear model on six proposals for the one-way shear strength of RC elements of different research groups [18]. The proposals were based on different hypotheses, and each one gave different specific weights to shear transfer actions. However, the shear transfer actions that influence the shear strength of a slender RC beam are widely recognised, which are: shear stresses over the depth of the (uncracked) compression zone due to flexion, interface shear transfer and residual tensile stresses across cracks, dowel action and the contribution of shear reinforcement (if it exists) [19].

One of the six proposals for the new One-Way Shear Equations 318 Building Code is based on the CCCM [20], and takes into account all the above-mentioned shear transfer actions [16], derived for design (code) purposes from a more complex model [21]. The CCCM shear strength predictions of the SMA shear-strengthened beams were supported by laboratory tests previously presented by the authors [9].

2.1. Compression chord Capacity model

The CCCM is a model based on the usual critical shear crack of elements both without shear reinforcement and with low and medium shear reinforcement (see Fig. 1a). This crack is composed of two branches described in [22,23]. A fundamental aspect of CCCM is its failure criterion as a result of loss of equilibrium triggered when the second branch of the critical crack is formed by a state of stresses in the bending compressed chord, which reaches the envelope described by Kupfer in [24] (see Fig. 1b). The stresses that develop in the compressed chord are: horizontal compressive stresses due to bending, shear stresses that can be simplified as shown in Fig. 1c, and vertical compression stresses (or "clamping stresses) produced by either the confinement of the shear reinforcement or external and active SMA shear-retrofit (see Fig. 1c).

Although the CCCM was not initially derived specifically as a model to consider externally added strengthening reinforcement, it can be used without causing problems. Therefore, the shear strength of an externally confined RC beam may be considered the sum of concrete contribution (V_{cu}), concrete contribution increment due to external confinement ($V_{cu}^{confinement}$) and shear reinforcement contribution (V_{su}). The main expressions governing shear strength are summarised in Table 1 for the particular case of RC beams with a rectangular cross-section. Material strength parameters adopted in Eqs. (1)-(9) are average laboratory values and not design values. See the notations for a description of each expression and all the factors.

Note that the CCCM can be useful for SMA-retrofits that confine only the compressed chord. This aspect was tested in the experimental study herein reported.

2.2. Shear strengthening of RC structures using the shape memory effect

The main shear strengthening topic of RC structures by means of SMAs using the shape memory effect is to take advantage of martensitic transformation [25] to generate recovery stresses to prestress RC structures. In this research, the prestressing technique was performed using Ni-Ti-Nb wires that wrapped RC beams in a transverse direction to strengthen beams, specifically in shear. These Ni-Ti-Nb wires were activated by a rise in temperature up to 200 °C through a heat gun that generated the reverse martensitic transformation.

The martensitic transformation took place within a finite interval of temperatures (Fig. 2) with a co-existence of two phases: austenite and martensite. The forward martensitic transformation was induced when cooling the austenite phase and consisted of the martensite phase appearing. If the temperature was appropriate for the material to be in the martensite phase, the reverse transformation was induced by heating the material. Note that this transformation exhibits thermal hysteresis: the forward and reverse transformations do not occur within the same temperature range. The SMA generates recovery stresses if the deformation is impeded during this reverse transformation. Furthermore, the

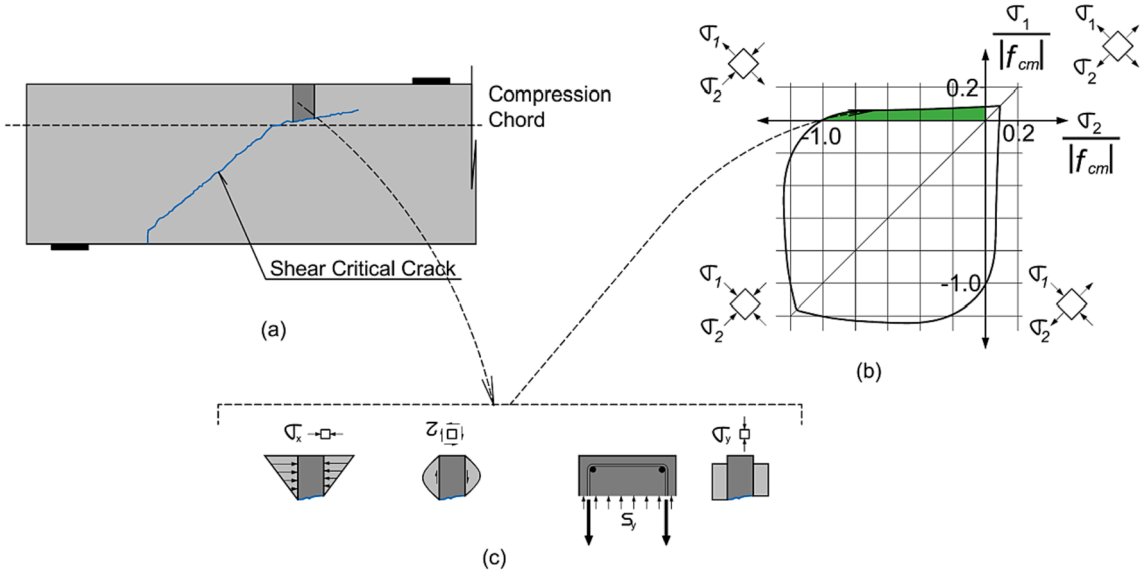

Fig. 1. Schematic of the failure criterion of the CCCM.

Table 1
Summary of the basic CCCM formulation particularised for reinforced concrete beams with rectangular cross-sections.

Equations	Expressions
Shear strength	$V_R = V_{cu} + V_{cu}^{confinement} + V_{su} \le V_{R,max} \quad V_{Rd} = V_{cu} + V_{su} \le V_{Rd,max}$ (1)
Strut crushing	$V_{Rd,max} = \alpha_{cw} b z \nu_1 f_{cd} \frac{\cot\theta + \cot\alpha}{1 + \cot^2\theta} \quad V_{Rd,max} = \alpha_{cw} b z \nu_1 f_{cd} \frac{\cot\theta + \cot\alpha}{1 + \cot^2\theta}$ (2)
Concrete contribution	$V_{cu} = 0.3\zeta \frac{x}{d} f_{cm}^{2/3} bd \not< V_{cu,min} = 0.25\left(\zeta K_c + \frac{20}{d_0}\right) f_{cm}^{2/3} bd \quad V_{cu} = 0.3\zeta \frac{x}{d} f_{cm}^{2/3} bd \not< V_{cu,min} = 0.25\left(\zeta K_c + \frac{20}{d_0}\right) f_{cm}^{2/3} bd \quad V_{cu} = 0.3\zeta \frac{x}{d} f_{cd}^{2/3} bd$ (3)
Concrete contribution increase due to confinement	$V_{cu}^{confinement} = \frac{A_{sw}}{s} f_s (d - x) \sin\alpha (\cot\theta + \cot\alpha) \Delta_{Vcu}$ (4)
Shear reinforcement	$V_{su} = \frac{A_{sw}}{s} f_s (d - x) \sin\alpha (\cot\theta + \cot\alpha) \quad V_{su} = \frac{A_{sw}}{s} f_{ywd} (d - x) \sin\alpha (\cot\theta + \cot\alpha)(1 + \Delta_{Vcu})$ (5)
Factors	**Expressions**
Size and slenderness effect	$\zeta = \frac{2}{\sqrt{1 + \frac{d_0}{200}}} \left(\frac{d}{a}\right)^{0.2}$ (6)
Relative neutral axis depth	$\frac{x}{d} = \alpha_e \rho_l \left(-1 + \sqrt{1 + \frac{2}{\alpha_e \rho_l}}\right)$ (7)
Non-dimensional confinement factor	$\Delta_{Vcu} = \zeta \frac{x}{d}$ (8)
Crack inclination	$\cot\theta = \frac{0.85d}{d - x} \le 2.5$ (9)

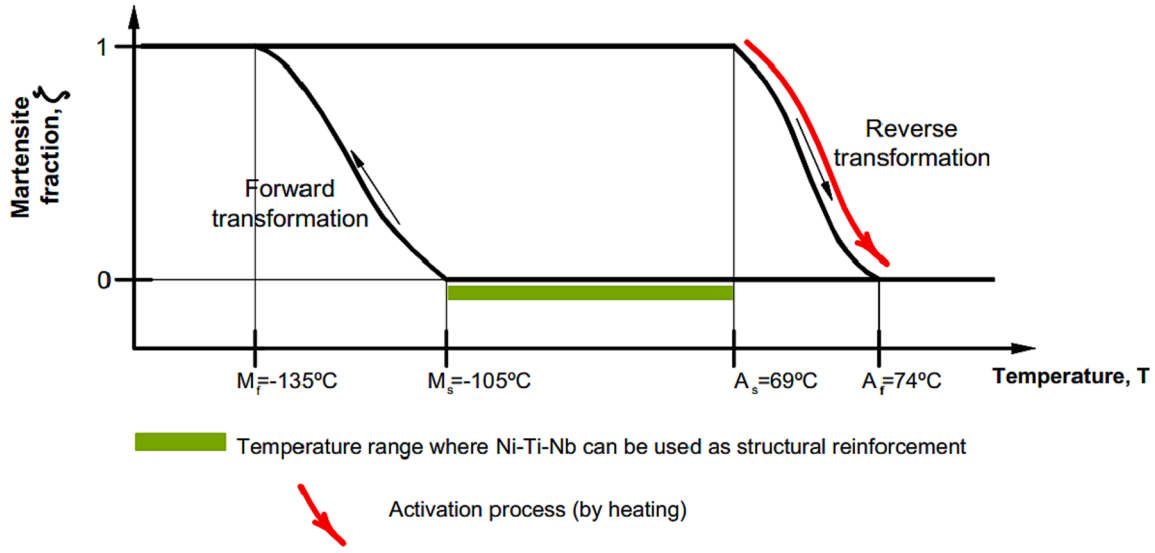

Fig. 2. Schematic of phase transformation for the first thermal cycle in Ni-Ti-Nb according to temperature.

wider the gap between those temperature intervals, the more likely the recovery stress generated after the subsequent cooling process to ambient temperature remain. This is a key aspect to consider when selecting SMAs to strengthen civil engineering structures, as the temperatures range for SMA performance has to include the usual range of civil engineering applications [26].

If an SMA is employed as external reinforcement to, for example, wrap a beam, and the recovery strain when heating and cooling is later constrained, the SMA generates recovery stresses by prestressing and/or confining the concrete member. The use of Ni-Ti-Nb wires as prestressing reinforcement for shear critical RC beams may overcome the limitation of a narrow hysteresis of other alloys, such as Ni-Ti.

In the presented strengthening technology, one important issue is to develop recovery stress with non-ideal initial geometry (non-straight wire) during the installing process or while activating SMA components. The evolution of expected recovery stresses in the presence of an initial gap and initial imperfection involved in the contact between concrete surface and wires can be reduced, and reinforcement effectiveness could be affected or directly disabled [27], as seen later.

3. Experimental study

3.1. Experimental program outline

This paper presents a new experimental study on ten small-scale beam specimens to complete the research published in [9] using the same materials. In this way, and by considering the previous and newly tested beams, the whole experimental program consisted of failure tests on 20 reinforced concrete (RC) small- scale beam specimens, all of which with the same geometry, no internal stirrups, and same longitudinal reinforcement composed of φ16 mm ($A_s = 201$ mm^2) standard B500SD rebar (both ends of the bar were welded to a plate to guarantee adequate anchorage), albeit different shear strengthening methods. The cast of beams was done in two different concrete batches. The results of the first phase of beams (continuous rectangular spiral of external Ni-Ti-Nb wires with a different pitch and a distinct load history) were discussed in [9], but are summarised in this paper to be compared to those of the second phase. The second phase consisted of testing beams with other shear strengthening configurations apart from continuous rectangular spiral (U-shape stirrups and variants of continuous rectangular spiral). The results of the second phase tests are herein presented, along with a comparative analysis of the results obtained in the two phases.

3.2. Designing test specimens

The new ten small scale RC beam specimens were produced from a single concrete batch, all with the same geometry and longitudinal reinforcement. The envisaged concrete compressive strength was 40 MPa. The RC beam specimens were 80-mm wide (b) and 150-mm deep (h), as shown in Fig. 3. The total length of the beam specimens was 900 mm, and tests were carried out by loading beams at a central point. The shear span, a, equalled 340 mm, with a/d approximately equal to 2.68, where d is the effective beam depth ($d = 127$ mm). The characteristics of beam specimens are summarised in Table 2.

The nomenclature for the different beam specimens (e.g., 7.1 - Sϕ3/100/UCR/A/G) continues the nomenclature employed for the first phase: it begins with a short test code (6.1 to 10.2) for fast identification purposes. To ensure the repeatability of findings, two identical beams were tested for each criteria phase (e.g., beams 7.1 and 7.2, where the second number indicates the first and the second tested beam specimens). Next, Sϕ3 (3-mm diameter spiral) or Uϕ3 (3-mm diameter U-shape stirrup) indicates the type of shear strengthening used, followed by "100" or "075", which indicates the pitch in mm of the Ni-Ti-Nb continuous rectangular spiral or stirrups spacing. The following field consists of three letters that may be, "UCR", "PCR" or "COL" which denote that the beam specimen was uncracked, previously shear cracked, or collapsed (respectively) when the strengthening spiral or stirrups was placed and activated. The next term indicates whether the strengthening spiral or stirrup had been either activated before the beam test (A) or set, but not activated, before the beam test (NA). The last term indicates an additional specimen characteristic: if the lower spiral part is placed in a groove, this term is a (G). If the spiral only wraps the upper mid specimen part and confines only the compressed beam chord, this term is an (S); see Fig. 3. The construction process of specimens is included in [28].

3.3. Fabrication of test specimens: Concrete and steel properties

Beams were cast in a precast concrete plant. All the beams, cubes and

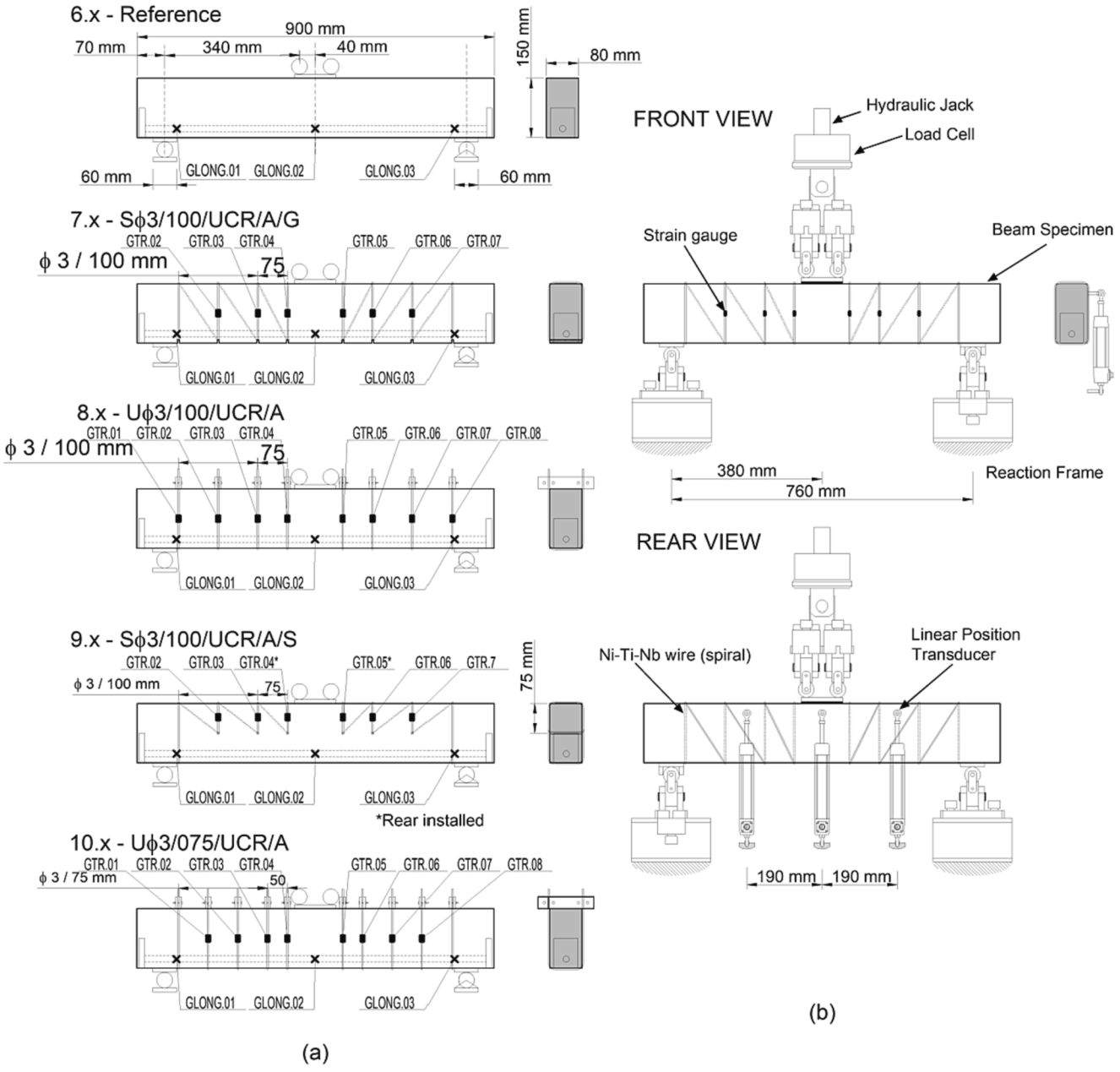

Fig. 3. **(a)** Beam geometry and strain-gauge positions of the beams tested in the second phase. **(b)** Test setup.

Table 2
Details of beam specimens.

Beam no.	Age at testing (days)	f_{cm} (MPa)	f_{sp} (MPa)	Shear strengthening				Comments
				ϕ/spacing (mm)	*Ni-Ti-Nb state*	φ_{front} (°)	φ_{back} (°)	
Beams tested in the first phase (already reported in [9]):								
1.1 – Reference	49	41.4	3.2	–	–	–	–	–
1.2 – Reference	56	41.7	3.2	–	–	–	–	–
2.1 - Sϕ3/100/UCR/A	63	41.9	3.2	ϕ3/100	Activated	90	56	Uncracked
2.2 - Sϕ3/100/UCR/A	68	42.1	3.2	ϕ3/100	Activated	90	56	Uncracked
3.1a - Sϕ3/100/UCR/NA	102	42.6	3.3	ϕ3/100	Non-Activated	90	56	Uncracked
3.1b - Sϕ3/100/COL/A	130	42.8	3.3	ϕ3/100	Activated	90	56	Tested after collapse 3.1a
3.2a - Sϕ3/100/UCR/NA	102	42.6	3.3	ϕ3/100	Non-Activated	90	56	Uncracked
3.2b - Sϕ3/100/COL/A	116	42.7	3.3	ϕ3/100	Activated	90	56	Tested after collapse 3.2a
4.1 - Sϕ3/100/PCR/A	175	43.0	3.3	ϕ3/100	Activated	90	56	Pre-cracked $V_{cr} = 17.79$ kN
4.2 - Sϕ3/100/PCR/A	182	43.0	3.3	ϕ3/100	Activated	90	56	Pre-cracked $V_{cr} = 18.08$ kN
5.1 - Sϕ3/075/UCR/A	263	43.2	3.4	ϕ3/75	Activated	90	63	Uncracked
5.2 - Sϕ3/075/UCR/A	272	43.2	3.4	ϕ3/75	Activated	90	63	Uncracked
Beams tested in the second phase (reported in this paper):								
6.1 – Reference	202	39.7	3.4	–	–	–	–	–
6.2 – Reference	202	39.7	3.4	–	–	–	–	–
7.1 - Sϕ3/100/UCR/A/G	279	39.8	3.5	ϕ3/100	Activated	90	56	Grooved
7.2 - Sϕ3/100/UCR/A/G	279	39.8	3.5	ϕ3/100	Activated	90	56	Grooved
8.1 - Uϕ3/100/UCR/A	224	39.7	3.4	ϕ3/100	Activated	90	90	U-shape
8.2 - Uϕ3/100/UCR/A	244	39.7	3.4	ϕ3/100	Activated	90	90	U-shape
9.1 - Sϕ3/100/UCR/A/S	272	39.8	3.5	ϕ3/100	Activated	90	37	Com. Chord confinement
9.2 - Sϕ3/100/UCR/A/S	279	39.8	3.5	ϕ3/100	Activated	90	37	Com. Chord confinement
10.1 - Uϕ3/075/UCR/A	321	39.8	3.5	ϕ3/075	Activated	90	90	U-shape
10.2 - Uϕ3/075/UCR/A	325	39.8	3.5	ϕ3/075	Activated	90	90	U-shape

cylinders of each phase were cast from a single batch. Maximum aggregate size of 14 mm was used. Standard 150-mm cubes and 150 mm × 300 mm cylinders were cast with specimens to obtain the compressive strength, f_{cm}, and the splitting strength, f_{sp}, respectively. These cubes and cylinders were left under the same environmental conditions as the beam specimens in the laboratory at a typical temperature of about 20 °C until the time beams were tested. The f_{cm} and f_{sp} estimations in Table 2 derive from the results of 26 cube tests for the compressive strength and 30 cylinder tests for splitting strength in compliance with Standards UNE-EN-12390–3 [29] and Standard UNE-EN-12390–6 [30], respectively, tested at 28 days (in compliance with EHE 2008 Code [31]) and at the age of each beam specimen upon testing.

Longitudinal reinforcement was composed of ϕ16 mm standard B500SD rebars ($A_s = 201$ mm^2). The mechanical properties of longitudinal bars, obtained in compliance with Standard UNE 36,065 [32], are: $f_y = 513$ MPa, $f_u = 642$ MPa, $\varepsilon_u = 20.5\%$ (the mean value of two reported tests).

3.4. SMA properties

The Ni-Ti-Nb wires used to prestress RC beams and their practical performance are presented in [9]. Briefly, the composition was Ti content at 45.81 at.%, Ni content at 45.76 at.% and Nb content at 8.43 at.%. Table 3 summarises the austenite and martensite properties of the Ni-Ti-Nb wires.

The provided material (6% initially prestrained by the manufacturer – red line in Fig. 4 a) was in the martensite phase at room temerature. After activation (heating process up to 200 °C), the austenite phase was induced and, if constraining was lacking, all deformation was recovered, denoted by the solid green line in Fig. 4 a (displaced for clarity). However, if the wire was perfectly constrained during activation, the maximum recovery stress took place, depicted by the solid blue line in Fig. 4 a. As the constraining process is not perfect when strengthening RC beams (see the picture in Fig. 4 a), with a remaining imperfection between 0% and 6%, the SMA wire recovers the strain due to initial imperfection (the green dashed line in Fig. 4 a, displaced for clarity) and develops partial recovery stress (the blue dashed line in Fig. 4 a). Afterwards, the beam test increases tensile stresses in SMA wires (the orange line in Fig. 4 a).

Table 3
Summary of the average thermo-mechanical properties of the Ni-Ti-Nb wires.

Property	Martensite	Austenite
E (GPa)	25	33
$f_{y,0.002}$ (MPa)	591	451
f_u (MPa)	1002	935
ε_u	0.37	0.55
σ^{Ms} (MPa)	–	494
σ^{Mf} (MPa)	–	543

To quantify recovery stresses under imperfect conditions, several wires with different initial imperfections were tested at [9], the adjustment presented by the authors to the tests for the prediction of recovery stresses σ_R [MPa] as a function of the initial imperfection i_0 [%] was $\sigma_{R(io)} = 7.6829\ i_0^2 + 443$ and a graphic summary of these results is presented in Fig. 4 b. The initial imperfection i_0 is determined by the ratio [%] between the actual (arch-shaped) length of the stirrup leg -solid line in Fig. 4 b schemes- and the straight line between the upper and lower clamps -discontinuous line in Fig. 4 b schemes-. Fig. 4 b shows, with empty black circles, the pairs of values (σ_R, i_o) obtained in characterization tests with initial imperfections, as the ones presented on the right in this figure, the imperfection range that affects the experimental study on RC beams (solid magenta line), the second-order parabola σ_R-i_0 adjustment previously described (small dashed lines), and the strain range for which the proposed equation for the prediction of recovery stresses is not valid since it is out of the range of the performed tests (big dashed lines). This analysis provided a good approximation of the recovery stresses at the SMA strengthening wires once the initial imperfection of the wire had been measured.

3.5. Strengthening of beam specimens

Different shear reinforcement configurations were used in the second phase to consider the distinct functional aspects of real RC beams. As this was done for the first phase, the prestrained Ni-Ti-Nb wire was wrapped around beam specimens and anchored and activated using a heat gun to produce reverse martensitic transformation. Therefore, unsuccessful in being shortened, the wire transmitted the stresses induced by its transformation to the beam by means of confining stresses, as previously

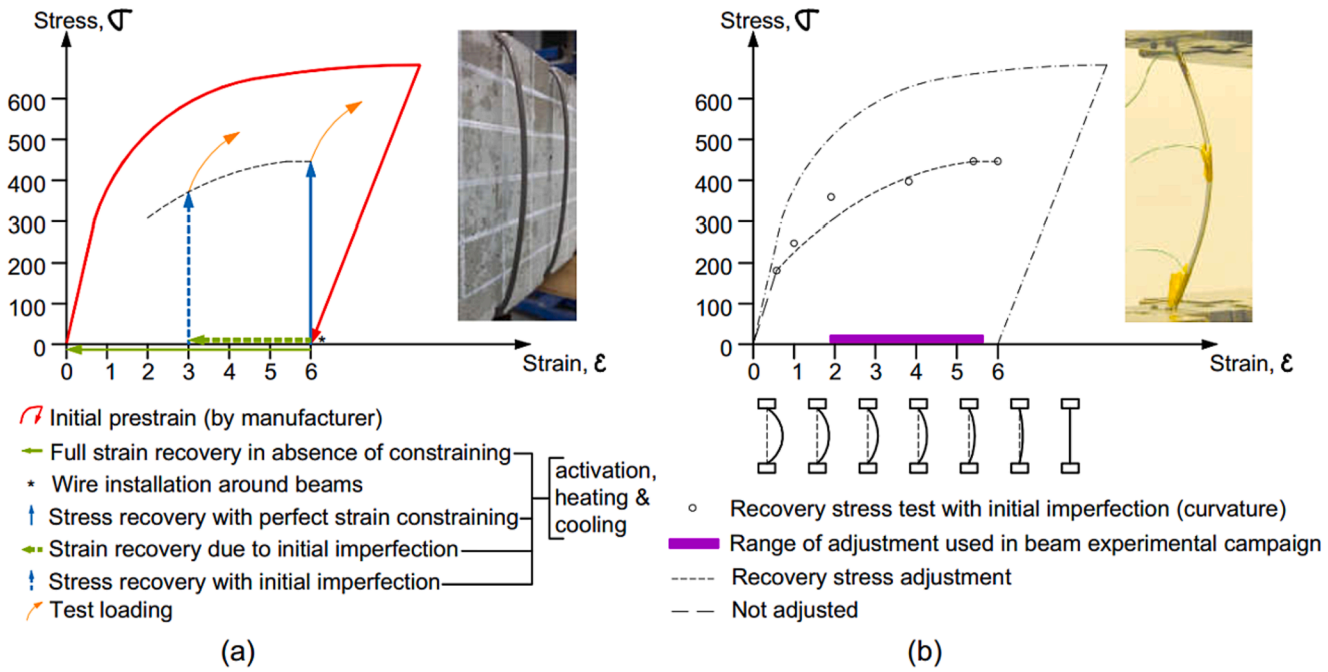

Fig. 4. a) Schematic stress–strain path of the Ni-Ti-Nb wires installed in the tested, strengthened RC beams and **b)** recovery stresses with different initial imperfections. .
Adapted from [9,27]

explained. The activation heat treatment for all beams (from both phases) was done employing a heat gun, ensuring, through the temporal attachment of K-type thermocouples, the prescribed temperature of 200 °C, optimum temperature observed in a previous characterisation of the utilised SMA.

Beams 6.1 and 6.2 were the reference beams, so no Ni-Ti-Nb external shear reinforcement was used. In all other beams, Ni-Ti-Nb reinforcement was activated before loading beams, which had not been pre-cracked. Beams 7.1 and 7.2 were indented with grooves in the lower part of each spiral (Fig. 5a,c) to test the influence on the dowel action of longitudinal reinforcement. Beams 8.1, 8.2, 10.1 and 10.2 were strengthened with Ni-Ti-Nb stirrups instead of spirals. Thus U-shape stirrups clamped in the upper part of the beams with bolted steel plates were used (Fig. 5b). Two different stirrup spacings were applied, i.e. 100 mm for beams 8.1 and 8.2, and 75 mm for beams 10.1 and 10.2. The beam configuration for beams 9.1 and 9.2 consisted of a continuous rectangular spiral strengthening only the compression chord of the beam (Fig. 5d). In this case, drilling the traverse direction of the beam had to

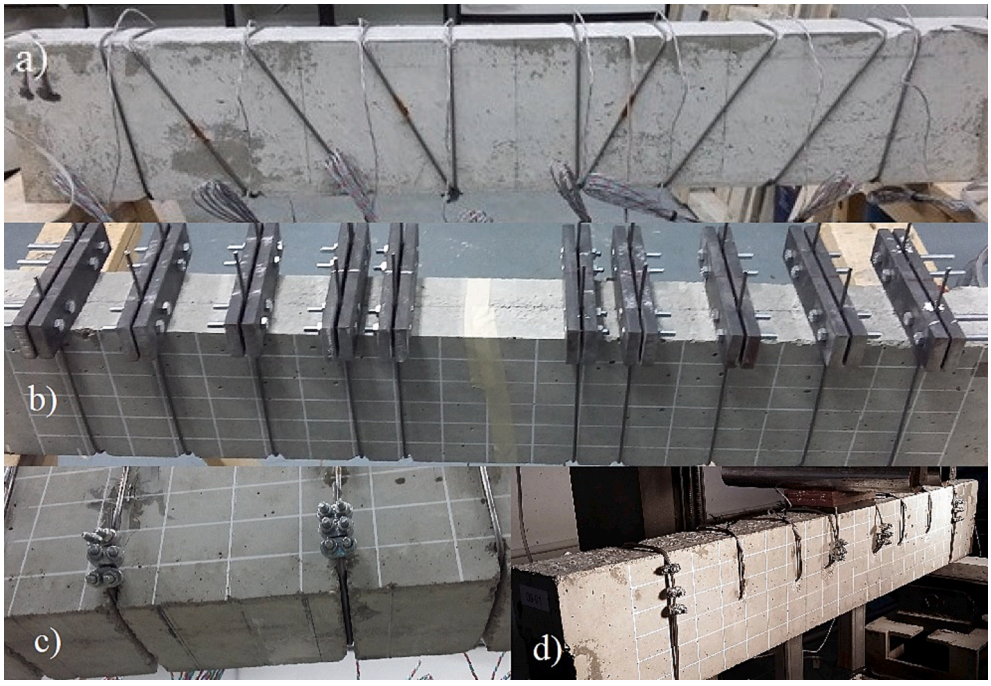

Fig. 5. a) Rear view of a beam strengthened by continuous rectangular spiral (beams 2.1 to 5.2). **b)** Beam strengthened by U-shape stirrups (8.1–8.2 and 10.1–10.2). **c)** Detail of grooves on a beam (7.1–7.2). **d)** Continuous rectangular spiral strengthen the compression chord of a beam (9.1–9.2).

be carried out to cross the beam with the Ni-Ti-Nb spiral continuously.

3.6. Instrumentation and testing procedure

To monitor the behaviour of the tested beam specimens, the applied load, the strains in reinforcement and displacements were measured using a load cell, strain gauges (see the locations in Fig. 3) and magnetostrictive transducers. Video and photography equipment were also employed to record the tests. All the parameters were monitored continuously by the data acquisition system.

Tests were carried out under displacement control with a hydraulic actuator and a maximum load capacity of 100 kN. The supporting plates were 60 mm long in the beams' longitudinal axis direction, and the loading plate was 105 mm wide. Two cylinders applied the load with centres spaced 80 mm apart. A sliding pin bearing was placed on the west side, and a fixed pin bearing on the east side (Fig. 3). The displacement at the loading plate was monotonically increased during the test.

4. Results of the experimental tests and discussion

4.1. Observed behaviour and shear strength of the tested beams

All the tested beams failed in shear, except one of the beams strengthened with a spiral pitch of 75 mm (beam 5.2), which failed on bending. Table 4 summarises the most important results of all the tested beams and shows in the last column ($V_{test}/V_{no\ strength}$) the ratio between the shear force at failure of the strengthened element, V_{test}, and the average shear force at failure of the control beams without strengthening ($V_{no\ strength}$). The beams of the first phase and its results were presented in [9], and the main findings were:

1. Significant increment in the maximum shear force for the activated spirals vs the reference beams (between 35.41 kN and 35.95 kN for the activated shear strengthened beams; between 18.30kN and 18.41 kN for the reference beams) and deflections at the maximum shear force (between 4.26 and 4.94 mm of deflection at the point load in the strengthened beams and of 1.59 and 1.64 mm in the reference beams)
2. The highest shear strengths were reached in the beams with the reduced pitch of 75 mm (shear strengths of 37.04 kN and 40.21 kN)
3. The effect of non-activated shear strengthening tested in the pre-loading tests was negligible (shear strengths of 18.23 kN and 21.47 kN)
4. Post-failure deflection significantly incremented in the shear-strengthened beams (between 7.5 and 22 mm for the strengthened beams and up to 3 mm for the reference beams)
5. The shear strength of the retrofitted beams with previous shear-cracks, and even those that reached ultimate shear strength, was similar to the uncracked retrofitted beams, except from beam 3.1b that had been more deflected than the other beams after the collapse in the previous test 3.1a. Therefore, it underwent more initial damage, as observed in [9]

Based on some of these findings, the design of the second phase of the experimental program did not include either previously cracked beams or non-activated reinforcements.

Regarding the second phase of the experimental results, Fig. 6 shows the deflection-shear force curves of the reference beams (6.1 and 6.2), the beams with grooves (7.1 and 7.2), the strengthened beams with the

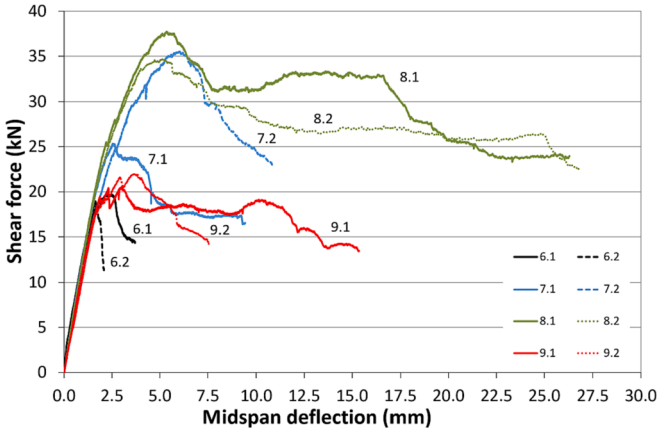

Fig. 6. Load vs deflection for the reference beams (6.1 and 6.2), the beams strengthened with grooved wires (7.1 and 7.2), the beams with U-shape stirrups (8.1 and 8.2), and the beams with spirals around their mid-upper part (9.1 and 9.2).

Table 4
Summary of the test results.

Beam no.	Age at testing (days)	f_{cm} (MPa)	f_{sp} (MPa)	V_{test} (kN)	δ at V_{test} (mm)	δ/l (1/l)	$V_{test}/V_{no\ strength}$
Beams tested in the first phase (already reported in [9])							
1.1 – Reference	49	41.4	3.2	18.30	1.59	1/479	–
1.2 – Reference	56	41.7	3.2	18.41	1.64	1/462	–
2.1 - Sϕ3/100/UCR/A	63	41.9	3.2	35.41	4.26	1/178	1.93
2.2 - Sϕ3/100/UCR/A	68	42.1	3.2	35.95	4.94	1/154	1.96
3.1a - Sϕ3/100/UCR/NA	102	42.6	3.3	18.23	1.67	1/456	–
3.1b - Sϕ3/100/COL/A	130	42.8	3.3	27.14	3.46	1/220	1.48
3.2a - Sϕ3/100/UCR/NA	102	42.6	3.3	21.47	1.69	1/450	–
3.2b - Sϕ3/100/COL/A	116	42.7	3.3	35.21	3.83	1/198	1.92
4.1 - Sϕ3/100/PCR/A	175	43.0	3.3	34.35	3.82	1/199	1.87
4.2 - Sϕ3/100/PCR/A	182	43.0	3.3	35.60	4.10	1/185	1.94
5.1 - Sϕ3/075/UCR/A	263	43.2	3.4	37.04	3.82	1/199	2.02
5.2 - Sϕ3/075/UCR/A	272	43.2	3.4	41.82	6.95	1/109	2.28
Beams tested in the second phase (reported in this paper):							
6.1 – Reference	202	39.7	3.4	19.71	2.50	1/303	–
6.2 – Reference	202	39.7	3.4	18.50	1.69	1/449	–
7.1 - Sϕ3/100/UCR/A/G	279	39.8	3.5	25.36	2.56	1/297	1.33
7.2 - Sϕ3/100/UCR/A/G	279	39.8	3.5	35.51	6.04	1/126	1.86
8.1 - Uϕ3/100/UCR/A	224	39.7	3.4	37.74	5.35	1/142	1.98
8.2 - Uϕ3/100/UCR/A	244	39.7	3.4	34.75	5.15	1/148	1.82
9.1 - Sϕ3/100/UCR/A/S	272	39.8	3.5	20.54	3.01	1/253	1.08
9.2 - Sϕ3/100/UCR/A/S	279	39.8	3.5	22.03	3.69	1/206	1.15
10.1 - Uϕ3/075/UCR/A	321	39.8	3.5	36.79	5.31	1/143	1.93
10.2 - Uϕ3/075/UCR/A	325	39.8	3.5	33.65	4.74	1/160	1.76

U-shape stirrups @ 100 mm (8.1 and 8.2) and the strengthened beams with the spirals wrapping their compression chord (9.1 and 9.2). We can see that these different strengthening methods were effective in all cases and gave similar values for the highest shear strengths with both continuous rectangular spiral (beam 7.2) and U-shape stirrups (8.1 and 8.2). The beams with only the confined compression chord (9.1 and 9.2) obtained lower strength values, but with significant increments in deflection. The unexpected low maximum load of 7.1 test was encountered and, although this result may not be considered representative, it should be noted that the critical shear crack started from one groove (close to the load point). So the critical crack developed along a shorter beam length and, consequently, mobilised fewer SMA branches (Fig. 7). However, this did not occur for beam 7.2, whose shear strength was similar to that of beams 4.1 and 4.2. As crack patterns affect shear strength, and grooves can affect crack patterns, as observed in beam 7.1, it would seem reasonable to avoid shear strengthening with grooves to avoid this variability.

The crack patterns in both the reference and strengthened beams were similar. Fig. 7 shows the crack patterns of all the tested beams immediately after the maximum applied load. For clarity sake, only one beam side, the critical one, is depicted. A typical shear crack pattern was detected for most tested beams, with a first and second branch of the critical shear crack. The developed first branch was inclined with an average value of 47°, but with relatively high scatter from around 30° to 60° from the lower beam part to the vicinity of the neutral axis. A second branch developed from the tip of the first branch to the point of load application and crossed the compression chord.

Regarding spiral wire reinforcement, no slippage around the corners of the cross-section, or damage to the wire anchorages, was detected.

Fig. 8 compares the deflection-shear force curves for the reference beams (6.1 and 6.2), the beams strengthened with U-shape stirrups spaced at 100 mm (8.1 and 8.2), and the beams with U-shape stirrups spaced at 75 mm (10.1 and 10.2). The behaviour of these beams, in maximum shear force and deflection terms, was similar. Note that the first branch of the shear critical cracks in each case started close to the lower part of a U-stirrup and passed through one U-stirrup, while the second branch of these cracks (flatter) passed through two U-stirrups upon the maximum load (see Fig. 7, beams 8.1, 8.2, 10.1 and 10.2) despite the different spacing.

Fig. 9 shows the strain measured in the longitudinal reinforcement of four representative tests (see the location of each strain gauge in Fig. 3). We can see that the longitudinal reinforcement in all the beams did not yield at the mid-span, but yielded at a load close to failure in the retrofitted beams at the position close to the support in the shear span.

The strains measured in the vertical segments of the Ni-Ti-Nb continuous rectangular spiral or U-stirrups are shown for a selection of representative beams in Fig. 10. For clarity sake, only the strains measured in the gauges located in the critical span are represented and the zero strain represents the situation immediately before the beam test; i.e. the activation process is not represented. The strain in the vertical links remained negligible until shear cracks propagated. Upon failure, different strain values were measured across the tested beams. Table 5 shows the strains ($\mu\varepsilon$) obtained at the maximum shear force for the links crossing the shear-critical crack (Fig. 7), and the average strain obtained from the arithmetic mean of the strains of the available gauge data at failure of the instrumented stirrup legs crossing the critical shear crack (these gauges are clearly indicated in Table 5 for each test).". The measured initial imperfection (i_o) after installing spirals or U-stirrups (before activation), and the estimated recovery stress after activation (σ_R), are also shown. Note that the Ni-Ti-Nb wires were prestressed thanks to the Shape Memory Effect (and the 6% strain previously defromed by the manufacturer) with initial stress after imperfect installation, with a minimum value of 316 MPa (see Table 5). The installation was handmade and no mechanically prestrain was applied to the SMA wires to avoid geometric imperfections during the installation process. The recovery stresses after the activation values (σ_R) were indirectly obtained by considering the initial imperfection (i_o) of each vertical segment and applying the performance curve shown in Fig. 4, as deduced in [9]. Moreover, by considering the tangent modulus of elasticity of Ni-Ti-Nb after recovery stresses were generated ($E = 25$ GPa), the increased stress in the Ni-Ti-Nb spiral was calculated from the average strain measured in the spiral legs crossing the critical crack upon the maximum load ($\Delta\sigma_\varepsilon = E{\cdot}\varepsilon$). The obtained stress increments per beam are also shown in Table 5. The final stress for maximum load appears in the last column ($\sigma_R + \Delta\sigma_\varepsilon$). Note that there is no bonding between the shear reinforcement and concrete, except for the friction concentrating in the corners of the cross-sections of beams. Note also that the increased stresses $\Delta\sigma_\varepsilon$ of Ni-Ti-Nb have not been considered for Tests 9.1 and 9.2 since the stirrups do not close the truss considered by Mörsch or the CCCM, that should wrap both the tensile longitudinal reinforcement and the resultant of the compressive stresses at the compression chord.

One important finding was that the new U-stirrups herein proposed were those with the lowest initial imperfection (i_o), and, therefore, the greatest initial stress to confine the RC element, as we can see in Table 5.

4.2. Comparative analysis of the beams with the whole confined cross-section

The main results of the whole experimental programme, except for tests 9.1 and 9.2, which are discussed in the next section, in average data terms are summarised in Table 6. The shear strength of the retrofitted beams was between 1.73 and 2.06 times (average 1.83) that of the reference beams (except for the beams in which only the compression chord was strengthened). The deflection for the maximum load of the retrofitted beams was higher by a factor of between 2.2 and 3.0 than that of the reference beams (average 2.6).

The two main different strengthening methods (continuous rectangular spiral and U-shape stirrups) with a different pitch or space between stirrups showed the effectiveness of our methodology, as depicted in Fig. 11. This figure compares the deflection-shear force curves for the beams of both phases: beams strengthened with continuous rectangular spiral (2.1, 2.2, 5.1 and 5.2) and those with U-shape stirrups (8.1, 8.2, 10.1 and 10.2). Non-significant differences were observed between spirals and U-stirrups in shear strength, as was slightly better ductility behaviour after shear failure for the U-stirrups.

The similar behaviour of the U-shaped stirrups and the spirals, despite the first system having fewer initial imperfections (from 0.45 to 0.64) than the second (from 0.94 to 2.66 -see Table 5-), may be due to the reduction of stresses produced by the initial imperfection is between 50 and 80 MPa (only a 30 MPa gap) within the mentioned ranges. This can be observed in the experimental values within the range of adjustment used in beam experimental program of Fig. 4b (in purple).

It should be noted that this initial imperfection range, which is useful in the Ni-Ti-Nb alloy used in this research, would be useless for other SMAs such as the Fe-Mn-Si-Cr-Ni alloy tested by the authors for the same purpose [7,8]. The reason for this is that the free shape recovery strain in the Ni-Ti-Nb alloy is 6% while in the Fe-Mn-Si-Cr-Ni alloy is around 1%, so, in most cases, during the activation of the Fe-Mn-Si-Cr-Ni alloy the initial imperfection would not be corrected and, therefore, recovery stresses would not develop.

5. Comparing the experimental results to the CCCM predictions

5.1. Predictions by CCCM

The predictions by CCCM and EC2 are presented in Table 7. Note that the shear strength predictions made by both CCCM and EC2 were deduced from the stresses based on the measurements indicated in Table 5 and the analysis presented in Fig. 4, while the shear strength design values by CCCM, also included in Table 7, were calculated with the stresses proposed for the SMA wires shown later in this paper.

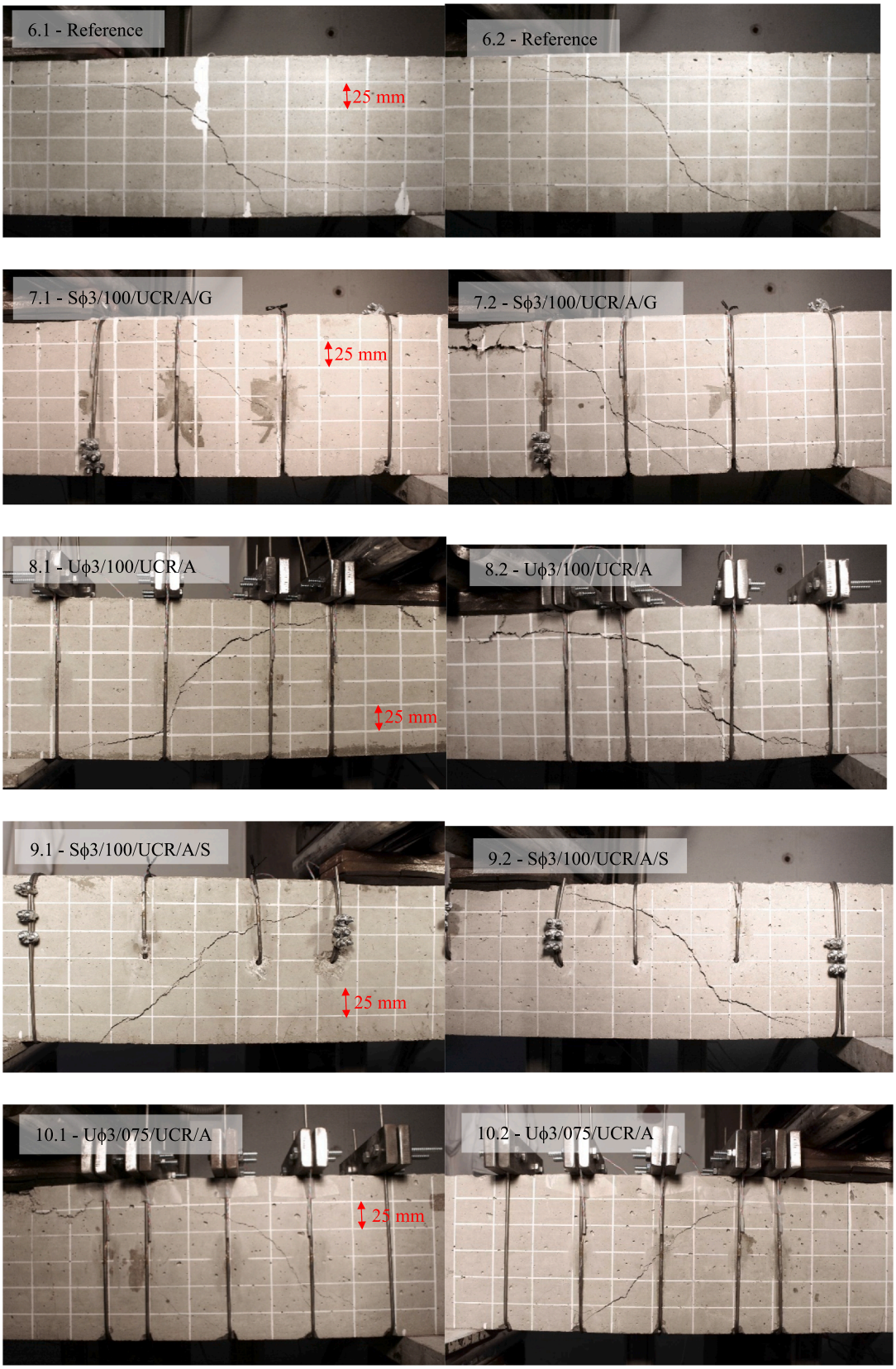

Fig. 7. Crack patterns immediately after their maximum load was achieved.

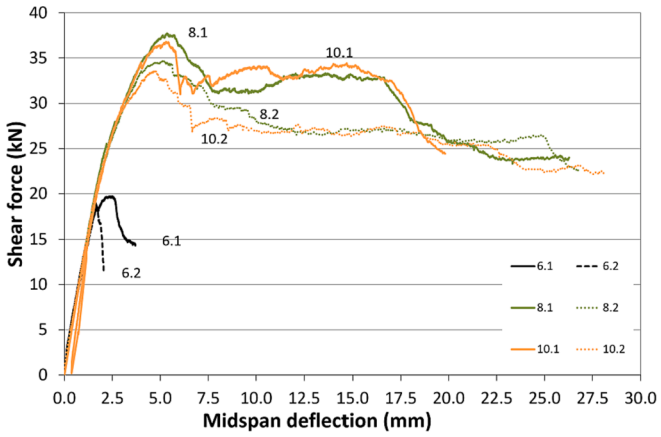

Fig. 8. Load vs deflection for the reference beams (6.1 and 6.2), the beams strengthened with U-shape stirrups with a pitch equalling 100 mm (8.1 and 8.2) and with a pitch equalling 75 mm (10.1 and 10.2).

The cylinder concrete compression strength, $f_{cm,cyl}$, was taken to equal 0.9 times that of the cube specimens, f_{cm} [31]. Compression strength varied slightly depending on specimen age upon testing, which non-significantly affected concrete contribution V_{cu} (Table 7).

No partial safety coefficients were used in the calculations presented in Table 7. The yield strength of the material, f_{ywd}, was substituted for the stress in the spiral upon failure (see f_s in Column 3 in Table 7). The pitch or spacing of the vertical segments of spirals or U-stirrups was constant in the tested beams (nominally 100 mm or 75 mm), except for the vertical segments closest to the loading plate (75 mm and 50 mm, see Fig. 5). For the CCCM application, nominal spacing was taken into account as it was the distance between the segments in the first branch of the critical crack [21], and it was the value required to obtain V_{su} (Table 7).

The predictions by the CCCM model with no modification with respect to the procedure established to evaluate internal reinforcement are satisfactory (see Table 7), with an average value of the V_{test}/V_{Rd} ratio equalling 1.14 and a 9.1% coefficient of variation for the two test phases. The average value of the V_{test}/V_{Rd} ratio was similar to the ratios of the shear strength of 784 RC beams without stirrups ($V_{test}/V_{Rd} = 1.17$) and 170 RC beams with stirrups ($V_{test}/V_{Rd} = 1.16$) [16]. Note that only the prediction of two beams, 3.1b - Sϕ3/100/COL/A and 7.1 - Sϕ3/100/UCR/A/G, was unsafe ($V_{test}/V_{Rd} < 1.0$). These beams cannot be considered representative due to the high damage level of the previous test in beam 3.1, and also to an unexpected low maximum load due to the modification made to the critical crack pattern cause by the groove, as previously mentioned in beam 7.1.

Furthermore, for the beams in which SMA reinforcement only wrapped the compression zone (beams 9.1 and 9.2), the V_{test}/V_{Rd} ratio values according to CCCM were 1.08 and 1.14, respectively, which were similar values to other beams. This was due to the initial derivation of CCCM, and the vertical compressive stresses in the compressed chord (on the second branch of the shear critical crack) were taken into account (see Fig. 1) to thus predict the shear strength of those beams retrofitted only on the upper part, and displayed the same reliability as the rest (with and without shear reinforcement in this case).

The predictions made when using the current Eurocode 2 [33] are also found in Table 7. Note that EC 2 presents two different models for the elements without and with stirrups: an empirical equation for the members without stirrups, and a variable angle truss model with no

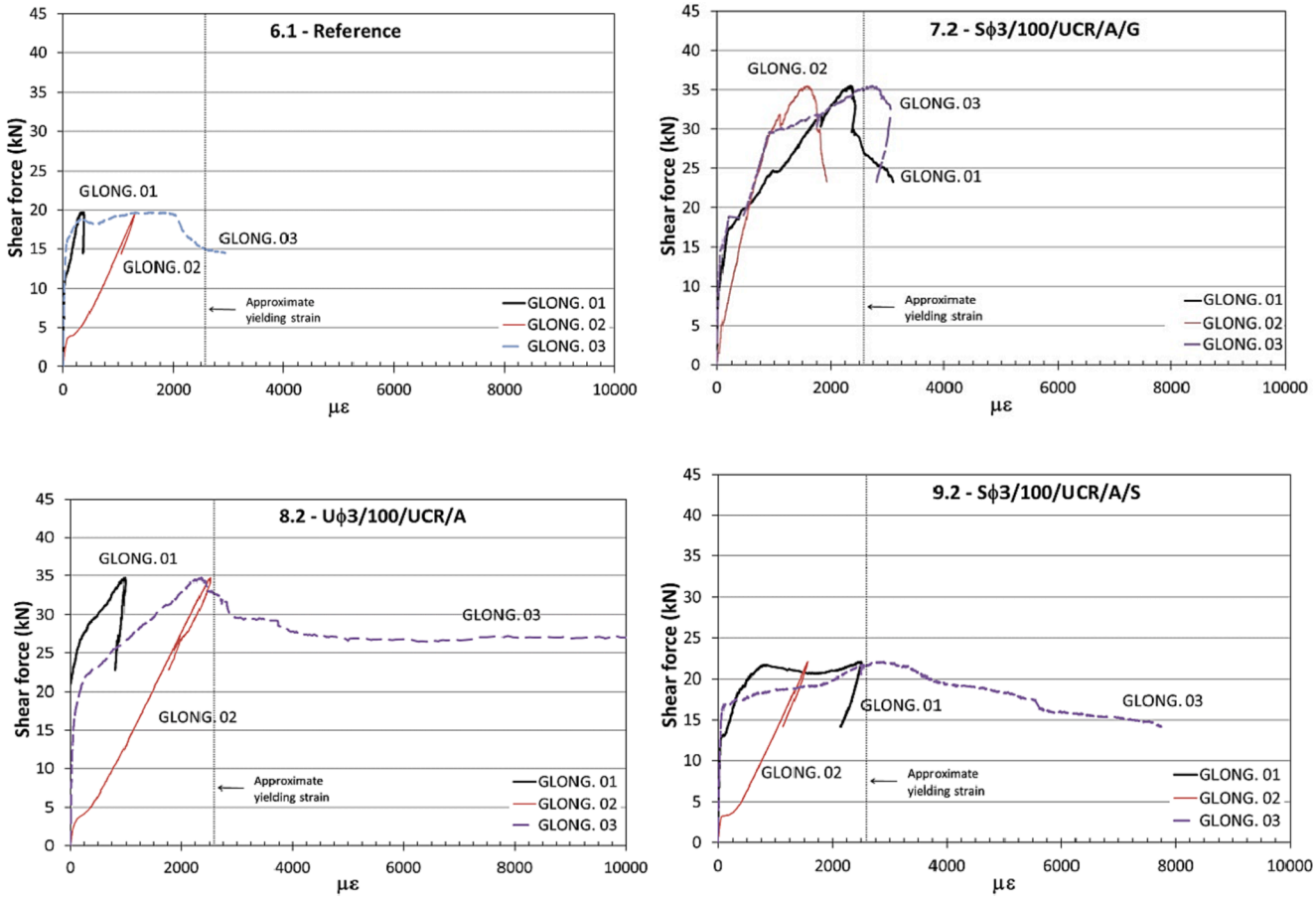

Fig. 9. Strains measured in the longitudinal reinforcement of beams 6.1, 7.2, 8.2 and 9.2.

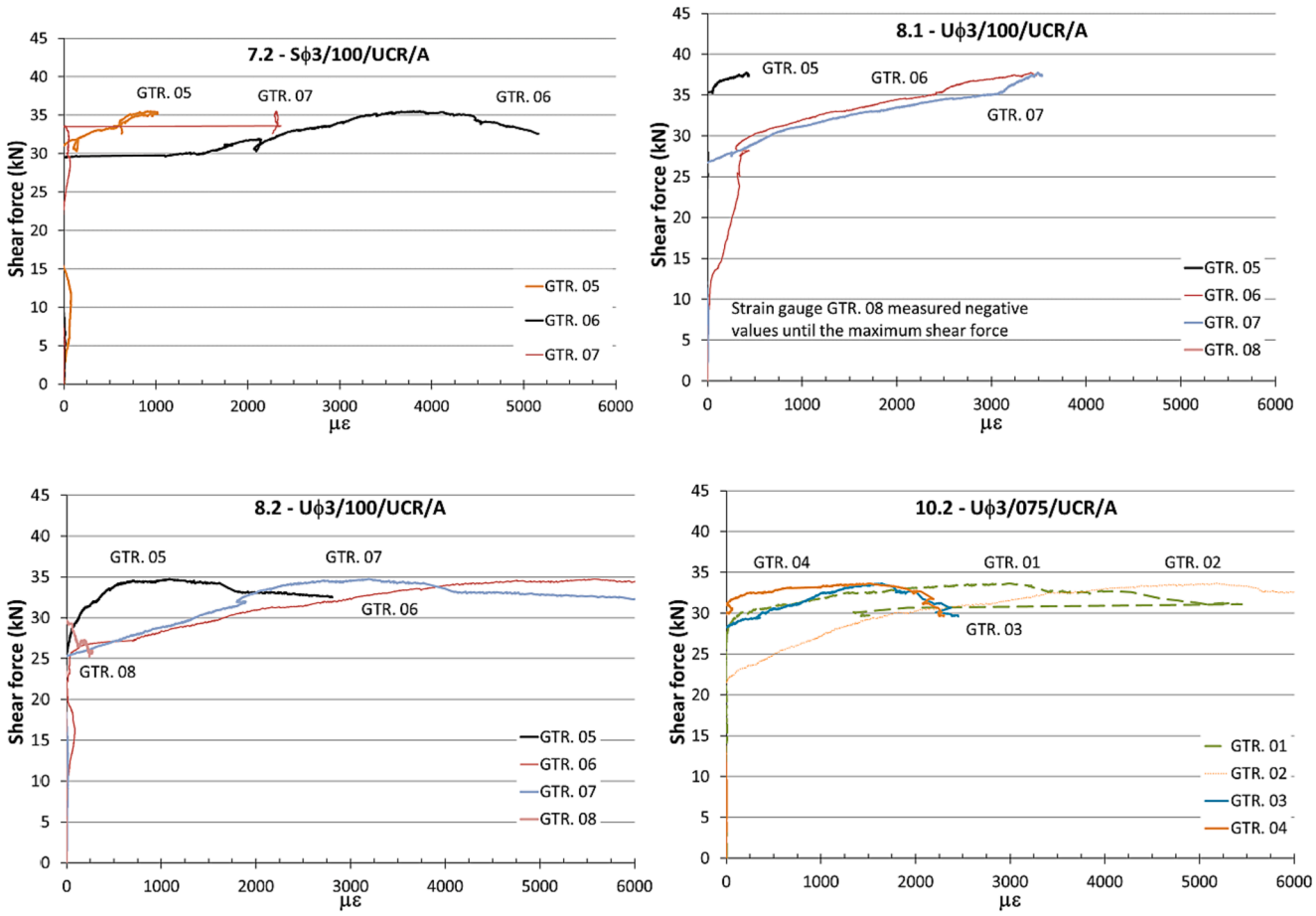

Fig. 10. Strains measured in the vertical segments of spirals or U stirrups in beams 7.2, 8.1, 8.2 and 10.2.

Table 5
Recovery stresses after activation with initial imperfection, the strains measured at the maximum shear force for the links crossing the shear-critical crack and all the developed stresses.

BEAM	i_o (%)	σ_R (MPa)	Gauges in the links crossing the critical crack				Average	$\Delta\sigma_\varepsilon$ (MPa)	$\sigma_R + \Delta\sigma_\varepsilon$ (MPa)
			GTR	$\mu\varepsilon$	GTR	$\mu\varepsilon$	$\mu\varepsilon$		
2.1	1.83	417	3	3148	–	–	3148	79	496
2.2	1.20	432	6	4645	7	4675	4660	116	548
3.1b	1.03	435	6	#	7	#	#	70*	505
3.2b	1.37	428	3	2016	–	–	2016	50	479
4.1	0.94	436	7	1968	–	–	1968	49	485
4.2	1.90	415	6	2686	–	–	2686	67	482
5.1	1.14	433	2	2371	–	–	2371	59	492
5.2**	1.00	435	7	–	–	–	–	–	–
7.1	2.66	389	6	1167	7	1711	1439	29	418
7.2	2.09	409	6	3870	–	–	3870	97	506
8.1	0.64	440	2	2207	3	3031	2619	55	495
8.2	0.53	441	6	5575	7	3191	4383	139	580
9.1	4.07	316	#	#	#	#	#	#	316
9.2	3.69	338	#	#	#	#	#	#	338
10.1	0.45	441	7	2794	8	1944	2369	70	511
10.2	0.53	441	2	5091	–	–	5091	127	568

No values were recorded due to a setup error
*Average value
** This beam failed in bending, so measurements are not significant

concrete contribution for the elements with stirrups. As this model did not intend to calculate the shear strength of the strengthened beam, the results are quite conservative and present high scatter, with an average V_{test}/V_{Rd} ratio value that equalled 1.45, and a 15.7% coefficient of variation for the two test phases.

Furthermore, the average × value, the neutral axis depth, was 49 mm according to Eq. (7). Fig. 7 shows that it is a very close estimation of the separation between the first branch of the critical crack (more vertical) and the second branch (more horizontal, through the compression chord). Note also that the CCCM hypothesised crack pattern (Fig. 1a) and the actual crack pattern (Fig. 7) are similar. For reference purposes, the spacing of the horizontal guidelines painted on the beam specimens

Table 6
Summary of the average test results of the whole experimental programme.

Beam type	V_{test} (kN)	δ at V_{test} (mm)	δ/l (1/l)	$V_{test}/V_{non\text{-}strengthened}$	Deflection increment (times)
Non-strengthened (1.1, 1.2, 3.1a, 3.2a, 6.1, 6.2)	19.10	1.80	1/433	–	–
Spiral pitch 100 mm (2.1, 2.2, 3.2b, 4.1, 4.2, 7.1, 7.2)	33.07	4.13	1/195	1.73	2.3
Spiral pitch 75 mm (5.1, 5.2)	39.43	5.38	1/154	2.06	3.0
Spirals (2.1, 2.2, 3.2b, 4.1, 4.2, 5.1, 5.2, 7.1, 7.2)	34.34	4.38	1/187	1.80	2.4
U-shape stirrup @100 mm (8.1, 8.2)	36.25	5.25	1/145	1.90	2.9
U-shape stirrup @ 75 mm (10.1, 10.2)	35.22	5.02	1/152	1.84	2.8
U-shape stirrups (8.1, 8.2, 10.1, 10.2)	35.73	3.98	1/225	1.87	2.2
100 mm spacing (2.1, 2.2, 3.2b, 4.1, 4.2, 7.1, 7.2, 8.1, 8.2)	33.70	4.35	1/185	1.76	2.4
75 mm spacing (5.1, 5.2, 10.1, 10.2)	37.33	5.20	1/165	1.95	2.9
Strengthened (with activation) (2.1, 2.2, 3.2b, 4.1, 4.2, 5.1, 5.2, 7.1, 7.2, 8.1, 8.2, 10.1 10.2)	34.74	4.59	1/176	1.82	2.6

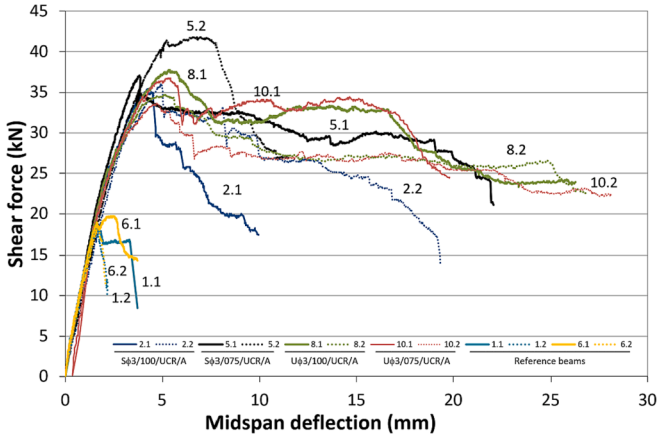

Fig. 11. Load vs. deflection for the reference beams, and the beams strengthened with spirals (2.1, 2.2, 5.1 and 5.2) and those with U-shape stirrups (8.1, 8.2, 10.1 and 10.2).

in Fig. 7 was 25 mm.

5.2. Design shear strength of the strengthened beams

After observing that the shear strength predictions by CCCM satisfactorily correlated with the experimental results, some simplifications were made for design purposes. Note that in the previous analysis, SMA stress was deduced from the measured imperfections and strains. For design purposes, the conservative recovery stresses for the strengthening wires (observed lower bound) were proposed. The following values are proposed:

- σ_R = 415 MPa. Value corresponding to an initial imperfection of 1.9% for spirals
- σ_R = 440 MPa. Value corresponding to an initial imperfection of 0.6% for U-shape stirrups
- σ_R = 400 MPa. Value corresponding to an initial imperfection of 2.4% for the spirals inside grooves in the lower beam parts
- σ_R = 315 MPa. Value corresponding to an initial imperfection of 4.1% for the spirals located in the compression chord of beams

A simplified design value is also proposed for stress increment of wires upon beam failure: strain increment equals 0.2%, which corresponds to an average increase of stresses upon failure equalling 50 MPa (as proposed in [9]), except for the spiral wrapping only the beam's compression chord, where a value of 0 MPa is proposed for the increment in stresses upon failure as the spiral is not crossed by the first branch of the critical crack. The yielding steel strength of the shear reinforcement in CCCM (f_s in Eq. (4)-(5)) and the E2 equations must be substituted by adding $\sigma_R + \Delta\sigma_\varepsilon$ for stress upon SMA active shear strengthening.

Both proposed design values, one for the initial recovery stress and another for the stress increment due to applied loads, are conservative (see Table 5). Note that the proposed initial imperfection can be considered an upper boundary for each configuration because the greater the retrofitted beam depth, less imperfection is produced during the assembly process. The use of small scale members makes it more difficult to place the wire around beams. U-shape stirrups are easier to place because the upper parts of links are not rounded and, thus, less imperfection is expected (Fig. 12).

The CCCM model showed, for design purposes, an average V_{test}/V_{Rd} ratio value that equalled 1.16 and a 9.5% coefficient of variation for the two test phases (Table 7). The results confirmed that, for design purposes, employing CCCM with the suggested stresses in strengthening wires offered accurate agreement with the tested elements. In any case, more research is necessary because other aspects were not considered, e.g. long-term wire relaxation or the actual strengthening effect on real scale beams.

5.3. Comparison made between the test results and CCCM and EC2 predictions

The results of the experimental program from the two beam test phases were also compared to those of the applied models. The main results of this comparison in average data terms are summarised in Table 8. This comparison was made by means of the ratio between the shear strength increment of the strengthened beams and the shear strength of the non-strengthened beams ($\Delta V_{strengthened}/V_{non\text{-}strengthened}$), expressed as percentages and referred to as the Shear Strength Index (SSI). This index can be obtained from the test results (SSI_{test}) and also from the predictions made by the different models, i.e. CCCM (SSI_{CCCM}) and EC2 (SSI_{EC2}). The ratios between the SSI of tests and of both CCCM (SSI_{test}/SSI_{CCCM}) and EC2 (SSI_{test}/SSI_{EC2}) were also obtained. These ratios indicated the goodness of each model for predicting increments in shear strength. As we can see in Table 8, CCCM showed greater precision in predicting these shear strength increments.

The correlation in both shear strength and shear strength increments terms between the CCCM predictions and the experimental results was more realistic than EC2 predictions, with SSI_{CCCM} = 83% and an average SSI_{test}/SSI_{CCCM} ratio = 1.00 for all the strengthened beams. Note SSI_{test} = 82%. The correlation for the EC2 predictions was SSI_{EC2} = 52% and an average SSI_{test}/SSI_{EC2} ratio = 1.58 for all the same strengthened beams. Note also that for the beams in which SMA only wrapped the compression zone, the CCCM predictions were satisfactory as SSI_{test} = 11% and SSI_{CCCM} = 14%. Thus CCCM correctly predicted the relative increments in shear strength for all the studied SMA strengthening systems, including the beams in which only the compression chord was strengthened. This aspect could not be studied with the EC2 shear strength equations. In any case, more research is necessary because other important aspects, such as the size effect that may affect this strengthening technology [34], have not been considered in this paper.

Table 7
Predictions by CCCM and EC 2.

Phase 1 beams	$f_{cm,cyl}$(MPa)	f_s(MPa)	V_{test}(kN)	Compression Chord Capacity Model	Eurocode 2								
				Prediction	Design								
				V_{cu}(kN)	V_{cu}^{conf}(kN)	V_{su}(kN)	V_{Rd}(kN)	V_{test}/V_{Rd}	V_{Rd}(kN)	V_{test}/V_{Rd}	$V_{Rd,c}$(kN)	$V_{Rd,s}$(kN)	V_{test}/V_{Rd}
1.1 – Reference	37.3	–	18.30	16.85	–	–	16.85	1.09	16.85	1.09	15.34	–	1.19
1.2 – Reference	37.5	–	18.41	16.92	–	–	16.92	1.09	16.92	1.09	15.37	–	1.20
2.1 - Sϕ3/100/UCR/A	37.7	496	35.41	16.96	4.19	8.45	29.60	1.20	28.81	1.23		20.56	1.72
2.2 - Sϕ3/100/UCR/A	37.9	548	35.95	17.01	4.62	9.34	30.88	1.16	28.86	1.25		22.73	1.58
3.1a - Sϕ3/100/UCR/NA	38.3	–	18.23	17.12	–	–	17.12	1.06	17.12	1.06	15.48	–	1.18
3.1b - Sϕ3/100/COL/A	38.5	505	27.14	17.17	4.25	8.61	30.03	0.90	29.01	0.94		20.94	1.30
3.2a - Sϕ3/100/UCR/NA	38.3	–	21.47	17.12	–	–	17.12	1.25	17.12	1.25	15.48	–	1.39
3.2b - Sϕ3/100/COL/A	38.4	479	35.21	17.14	4.03	8.15	29.34	1.20	28.99	1.21		19.86	1.77
4.1 - Sϕ3/100/PCR/A	38.7	485	34.35	17.21	4.08	8.27	29.57	1.16	29.05	1.18		20.13	1.71
4.2 - Sϕ3/100/PCR/A	38.7	482	35.60	17.21	4.06	8.22	29.50	1.21	29.05	1.23		20.01	1.78
5.1 - Sϕ3/075/UCR/A	38.9	492	37.04	17.25	5.49	11.11	33.86	1.09	32.94	1.12		27.49	1.35
5.2 - Sϕ3/075/UCR/A	38.9	505	41.85	17.25	5.63	11.41	34.30	1.22	32.94	1.27		28.22	1.48
Phase 2 beams													
6.1 – Reference	35.73	–	19.71	16.47	–	–	16.47	1.20	16.47	1.20	15.12	–	1.30
6.2 – Reference	35.73	–	18.50	16.47	–	–	16.47	1.12	16.47	1.12	15.12	–	1.22
7.1 - Sϕ3/100/UCR/A/G	35.82	418	25.36	16.49	3.55	7.12	27.16	0.90	27.97	0.91	–	17.22	1.47
7.2 - Sϕ3/100/UCR/A/G	35.82	506	35.51	16.49	4.29	8.62	29.40	1.21	27.97	1.27	–	20.85	1.70
8.1 - Uϕ3/100/UCR/A	35.73	495	37.74	16.47	3.76	7.56	27.79	1.36	27.67	1.36	–	20.00	1.89
8.2 - Uϕ3/100/UCR/A	35.73	580	34.75	16.47	4.41	8.85	29.73	1.17	27.67	1.26	–	23.43	1.48
9.1 - Sϕ3/100/UCR/A/S	35.82	316	20.54	16.49	2.61	–	19.10	1.08	19.10	1.08	15.14	–	1.36
9.2 - Sϕ3/100/UCR/A/S	35.82	338	22.03	16.49	2.80	–	19.29	1.14	19.10	1.15	15.14	–	1.46
10.1 - Uϕ3/075/UCR/A	35.82	511	36.79	16.49	5.19	10.40	32.08	1.15	31.43	1.17	–	27.53	1.34
10.2 - Uϕ3/075/UCR/A	35.82	568	33.65	16.49	5.76	11.56	33.81	1.00	31.43	1.07	–	30.60	1.10
					Average	1.14		1.16			1.45		
					Standard deviation	0.10		0.11			0.23		
					Coeff. of Variation (%)	9.1		9.5			15.7		

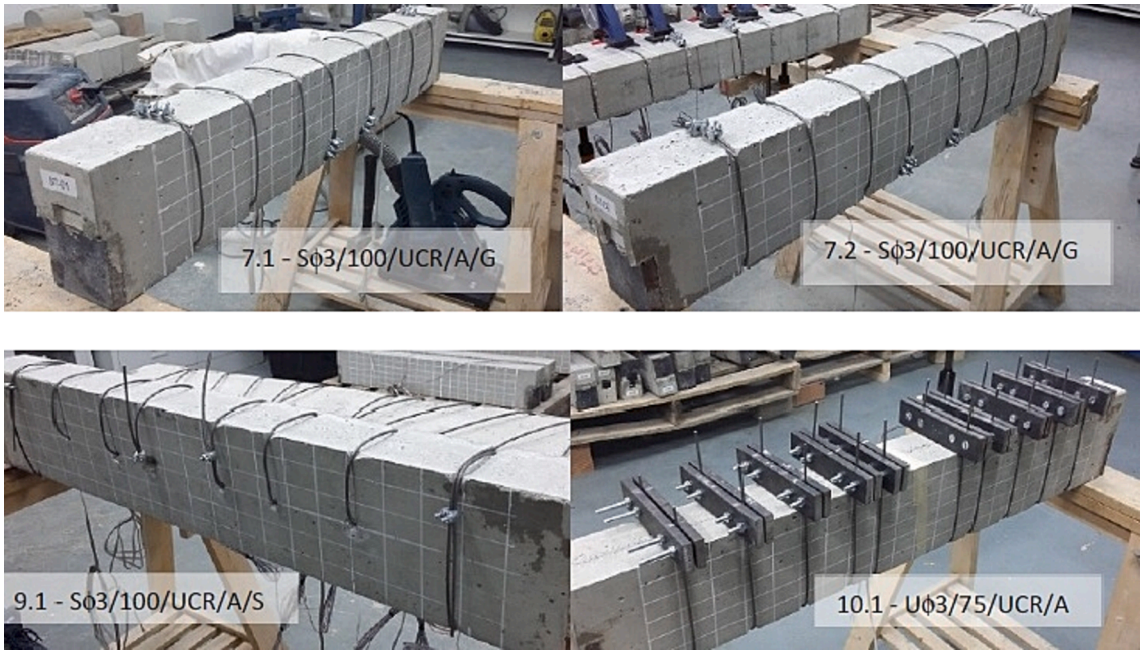

Fig. 12. Beams during wire installation (initial imperfection before activation).

Table 8
Summary of the comparison values of the two experimental program phases and predictions.

Average beams with…	Experimental		CCCM				EC2			
	V_{test} (kN)	SSI_{test} (%)	V_{CCCM} *(kN)*	$\frac{V_{test}}{V_{CCCM}}$	SSI_{CCCM} (%)	$\frac{SSI_{test}}{SSI_{CCCM}}$	V_{EC2} *(kN)*	$\frac{V_{test}}{V_{EC2}}$	SSI_{EC2} (%)	$\frac{SSI_{test}}{SSI_{EC2}}$
Non-strengthened (1.1, 1.2, 3.1a, 3.2a, 6.1, 6.2)	19.10	–	16.82	1.14	–	–	15.32	1.25	–	–
Spirals (2.1, 2.2, 3.2b, 4.1, 4.2, 5.1, 5.2, 7.2)	34.34	80	30.37	1.13	80	0.99	22.30	1.54	46	1.75
U-shape stirrups (8.1, 8.2, 10.1, 10.2)	35.73	87	30.85	1.16	83	1.04	25.39	1.41	66	1.32
100 mm spacing (2.1, 2.2, 3.2b, 4.1, 4.2, 7.2, 8.1, 8.2)	33.70	76	29.54	1.14	76	1.01	20.94	1.61	37	2.08
75 mm spacing (5.1, 5.2, 10.1, 10.2)	37.33	95	33.50	1.11	99	0.96	28.45	1.31	86	1.11
Strengthened (2.1, 2.2, 3.2b, 4.1, 4.2, 5.1, 5.2, 7.2, 8.1, 8.2, 10.1, 10.2)	34.74	82	30.76	1.13	83	0.99	23.25	1.49	52	1.58
Wrapping comp. chord (9.1, 9.2)	21.29	11	19.19	1.11	14	0.81	15.32	1.39	0	0

6. Conclusions

An experimental study involving 10 small-scale beam specimens is presented to study different active SMA external shear strengthening configurations: with U-shaped stirrups to facilitate the construction process, and with spirals whose lower part is arranged in the grooved RC element, and also by spirally confining the compressed chord. The results were also compared to those obtained in a previous experimental study that involved 10 other beam specimens, with the same dimensions and materials, but with different strengthening configurations. The experimental shear strengths were compared in detail to the predictions made by CCCM and EC2.

The main drawn conclusions are:

- The experimental results show promising performance for the proposed technology, which increases both the shear strength of the retrofitted beams and deflection upon failure. On average, the retrofitted beams with active strengthening (in all their depths) show an 82% increment in shear strength and 2.6-fold greater deflections
- The new proposed U-stirrups are those with the least initial imperfection (i_o) and, therefore, with higher initial stress to confine the RC element. In any case, the beams strengthened with U-stirrups offer non-significant differences with those with active spirals in shear strength terms, however display slightly better ductility behaviour after shear failure
- Grooves affect the crack pattern by also affecting the retrofitted RC element's shear behaviour and introducing undesired variability. In addition, the spiral retrofit with grooves offers no improvement in relation to the spiral retrofits without grooves. This conclusion must be taken cautiously given the very few tests conducted in the beams with grooves
- The beams with only the confined compression chord have lower shear strength values than the other active retrofits, but significant increments in deflection after the peak shear force
- The predictions by CCCM with no modifications in relation to the original procedure for standard RC beams, and by taking into account the stress deduced at SMA wires (from the measures taken before and during tests), are satisfactory with an average V_{test}/V_{Rd} ratio value that equals 1.14 and a 9.1% coefficient of variation for the 20 analysed tests. Furthermore for design purposes, the CCCM model shows an average V_{test}/V_{Rd} ratio value that equals 1.16 and a 9.5% coefficient of variation. These results confirm that using CCCM for design purposes with the suggested stresses in strengthening wires offers a safe (V_{test}/V_{pred} ratios range from 0.9 to 1.36) and accurate (V_{test}/V_{pred} standard deviation is 0.11) agreement with the tested elements. In any case, more research is necessary because other important aspects, such as size effect, are not considered
- The EC2 predictions are quite conservative and present high scatter, with an average V_{test}/V_{Rd} ratio value equalling 1.45, and a 15.7% coefficient of variation for the studied beams

- The correlation in terms of the shear strength increment between the CCCM predictions and the experimental results is accurate. Thus CCCM correctly predicts the relative increment of shear strength for all the studied SMA strengthening systems, including the beams in which only the compression chord was strengthened. This aspect could not be studied with the EC2 shear strength equations

CRediT authorship contribution statement

Joan M. Rius: Conceptualization, Writing – original draft. **Antoni Cladera:** Conceptualization, Supervision. **Benito Mas:** Conceptualization. **Carlos Ribas:** Conceptualization, Writing – original draft, Supervision.

Declaration of Competing Interest

The authors declare that they have no known competing financial interests or personal relationships that could have appeared to influence the work reported in this paper.

Acknowledgements

This research was conducted as part of research projects RTI2018-099091-B-C22 by MCIN/AEI/10.13039/501100011033 and by "ERDF A way of making Europe" and BIA2015-64672-C4-3-R (AEI / FEDER, UE). Beam specimens were cast in the Pastor precast concrete plant, located in Santa Margalida (Majorca, Spain). The authors acknowledge their help and assistance.

References

[1] Adhikary BB, Mutsuyoshi H. Shear strengthening of reinforced concrete beams using various techniques. Constr Build Mater 2006;20:366–73. https://doi.org/10.1016/j.conbuildmat.2005.01.024.
[2] Guo R, Ren Y, Li M, Hu P, Du M, Zhang R. Experimental study on flexural shear strengthening effect on low-strength RC beams by using FRP grid and ECC. Eng Struct 2021;227:111434. https://doi.org/10.1016/j.engstruct.2020.111434.
[3] Colajanni P, Recupero A, Spinella N. Increasing the shear capacity of reinforced concrete beams using pretensioned stainless steel ribbons. Struct Concr 2017;18:444–53. https://doi.org/10.1002/suco.201600089.
[4] Motavalli M, Czaderski C, Pfyl-Lang K. Prestressed CFRP for strengthening of reinforced concrete structures: recent developments at empa. Switzerland J Compos Constr 2011;15:194–205. https://doi.org/10.1061/(ASCE)CC.1943-5614.0000125.
[5] Soroushian P, Ostowari K, Nossoni A, Chowdhury H. Repair and strengthening of concrete structures through application of corrective posttensioning forces with shape memory alloys. Transp Res Rec J Transp Res Board 2001;1770(1):20–6.
[6] Zerbe L, Reda M, Dawood M, Belarbi A, Senouci A, Gencturk B, et al. Behavior of Retrofitted Concrete Members Using Iron-Based Shape Memory Alloys. SMAR 2017- Fourth Conf. Smart Monit. Assesment Rehabil. Civ. Struct., Zuruch: 2017, p. 9.
[7] Montoya-Coronado LA, Ruiz-Pinilla JG, Ribas C, Cladera A. Experimental study on shear strengthening of shear critical RC beams using iron-based shape memory alloy strips. Eng Struct 2019;200:109680. https://doi.org/10.1016/j.engstruct.2019.109680.
[8] Cladera A, Montoya-Coronado LA, Ruiz-Pinilla JG, Ribas C. Shear strengthening of slender reinforced concrete T-shaped beams using iron-based shape memory alloy strips. Eng Struct 2020;221:111018. https://doi.org/10.1016/j.engstruct.2020.111018.
[9] Rius JM, Cladera A, Ribas C, Mas B. Shear strengthening of reinforced concrete beams using shape memory alloys. Constr Build Mater 2019;200:420–35. https://doi.org/10.1016/j.conbuildmat.2018.12.104.
[10] Shahverdi M, Czaderski C, Annen P, Motavalli M. Strengthening of RC beams by iron-based shape memory alloy bars embedded in a shotcrete layer. Eng Struct 2016;117:263–73. https://doi.org/10.1016/j.engstruct.2016.03.023.
[11] Shahverdi M, Michels J, Czaderski C, Motavalli M. Iron-based shape memory alloy strips for strengthening RC members: material behavior and characterization. Constr Build Mater 2018;173:586–99. https://doi.org/10.1016/j.conbuildmat.2018.04.057.
[12] Izadi MR, Ghafoori E, Shahverdi M, Motavalli M, Maalek S. Development of an iron-based shape memory alloy (Fe-SMA) strengthening system for steel plates. Eng Struct 2018;174:433–46. https://doi.org/10.1016/j.engstruct.2018.07.073.
[13] Abouali S, Shahverdi M, Ghassemieh M, Motavalli M. Nonlinear simulation of reinforced concrete beams retrofitted by near-surface mounted iron-based shape memory alloys. Eng Struct 2019;187:133–48. https://doi.org/10.1016/j.engstruct.2019.02.060.
[14] Karayannis CG, Chalioris CE. Shear tests of reinforced concrete beams with continuous rectangular spiral reinforcement. Constr Build Mater 2013;46:86–97. https://doi.org/10.1016/j.conbuildmat.2013.04.023.
[15] Mas B, Cladera A, Ribas C. Experimental study on concrete beams reinforced with pseudoelastic Ni-Ti continuous rectangular spiral reinforcement failing in shear. Eng Struct 2016;127:759–68.
[16] Cladera A, Marí A, Bairán JM, Ribas C, Oller E, Duarte N. The compression chord capacity model for the shear design and assessment of reinforced and prestressed concrete beams. Struct Concr 2016;17:1017–32. https://doi.org/10.1002/suco.201500214.
[17] Muttoni A, Schwartz J. Behaviour of beams and punching in slabs without shear reinforcement. IABSE Colloq 1991;62:703–8.
[18] Belarbi A, Kuchma DA, Sanders DH. Proposals for New One-Way Shear for the 318 Building Code. Concr Int 2017;39:29–32.
[19] ASCE-ACI-Committee-445. Recent approaches to shear design of structural concrete. J Struct Eng 1998:1375–417.
[20] Cladera A, Marí A, Bairán J-M, Oller E, Ribas C. One-Way Shear Design Method Based on a Multi-Action Model. Concr Int 2017;39:40–6.
[21] Marí A, Bairán J, Cladera A, Oller E, Ribas C. Shear-flexural strength mechanical model for the design and assessment of reinforced concrete beams. Struct Infrastruct Eng 2015;11(11):1399–419.
[22] Zararis PD, Papadakis GC. Diagonal shear failure and size effect in RC beams without web reinforcement. J Struct Eng 2001;127:733–42. https://doi.org/10.1061/(ASCE)0733-9445(2001)127:7(733).
[23] Park H-G, Choi K-K, Wight JK. Strain-based shear strength model for slender beams without web reinforcement. ACI Struct J 2006;103:783–93.
[24] Kupfer HB, Gerstle KH. BEHAVIOR OF CONCRETE UNDER BIAXIAL STRESSES. vol. 99. 1973.
[25] Otsuka K, Wayman CM. Shape Memory Materials. United Kingdom: Cambridge University Press; 1998.
[26] Janke L, Czaderski C, Motavalli M, Ruth J. Applications of shape memory alloys in civil engineering structures - Overview, limits and new ideas. Mater Struct Constr 2005;38:578–92. https://doi.org/10.1617/14323.
[27] Lee WJ, Weber B, Leinenbach C. Recovery stress formation in a restrained Fe-Mn-Si-based shape memory alloy used for prestressing or mechanical joining. Constr Build Mater 2015;95:600–10. https://doi.org/10.1016/j.conbuildmat.2015.07.098.
[28] Rius JM. PhD Thesis: Active shear strengthening of RC beams using Ni-Ti-Nb shape memory alloys. University of the Balearic Islands; 2018.
[29] AENOR. UNE-EN-12390-3. Testing hardened concrete - Part 3: Compressive strength of test specimens 2009.
[30] AENOR. UNE-EN-12390-6. Testing hardened concrete - Part 6: Tensile splitting strength of test specimens 2010.
[31] Comisión Permanente del Hormigón. Instrucción de Hormigón Estructural EHE-2008. Madrid: Ministerio de Fomento; 2008.
[32] AENOR. UNE36065. Ribbed bars of weldable steel with special characteristics of ductility for the reinforcement of concrete 2011.
[33] European Committee for Standardization. Eurocode 2: Design of Concrete Structures: Part 1: General Rules and Rules for Buildings. European Committee for Standardization; 2002.
[34] Cladera Bohigas A, Montoya Coronado LA, Ruiz Pinilla JG, Ribas González CR. Refuerzo externo a cortante en vigas de hormigón mediante aleaciones con memoria de forma en base hierro: de la prueba de concepto a la escala real. Hormigón y Acero 2022;73:7–15. https://doi.org/10.33586/HYA.2020.2685.